Research Square

Preprints are preliminary reports that have not undergone peer review.
They should not be considered conclusive, used to inform clinical practice,
or referenced by the media as validated information.

# TREM2 Targeted $^{89}$Zr-ImmunoPET Visualizes Microglial Activation during the Inflammatory Response

**Evanta Kabir**
The University of Texas Health Science Center at Houston
**Önder Otlu**
The University of Texas Health Science Center at Houston
**Taylor M. Brinson**
The University of Texas Health Science Center at Houston
**Ronnie The Phong Trinh**
The University of Texas MD Anderson Cancer Center
**Wei Xiong**
The University of Texas Health Science Center at Houston
**Yaima L. Lightfoot**
The University of Texas MD Anderson Cancer Center
**William J. Ray**
The University of Texas MD Anderson Cancer Center
**Zhiqiang An**
The University of Texas Health Science Center at Houston
**Ningyan Zhang**
The University of Texas Health Science Center at Houston
**Federica Pisaneschi**
Federica.Pisaneschi@uth.tmc.edu
The University of Texas Health Science Center at Houston

**Article**

**Keywords:**

**Posted Date:** May 21st, 2026

**DOI:** https://doi.org/10.21203/rs.3.rs-9612465/v1

**License:** This work is licensed under a Creative Commons Attribution 4.0 International License. Read Full License

**Additional Declarations:** Competing interest reported. The UTHealth Houston Office of Technology has filed a patent application for novel TREM2-specific antibodies, naming Z.A. and N.Z. as inventors. F.P. is an Associate Editor of npj Imaging. She was not involved in the handling or editorial decision-making process of this manuscript. The remaining authors declare no competing interests.

# Abstract

Neuroinflammation is mainly mediated by activated immune cells such as microglia and astrocytes, and is a key driver of neurodegenerative and neurological diseases. Triggering receptor expressed on myeloid cells 2 (TREM2), which is selectively expressed on microglia in the central nervous system, has emerged as a promising target for assessing microglial activation. We developed an $^{89}$Zr-labeled bispecific anti-TREM2/anti-transferrin receptor antibody ($^{89}$Zr-T2BA). TREM2 specificity was assessed in vitro in wild-type (WT) and TREM2-overexpressing (TREM2 OE) HEK293T cells. In vivo specificity and diagnostic performance were evaluated in healthy WT and TREM2 knockout (KO) mice, and in a systemic lipopolysaccharide (LPS)-induced neuroinflammation model. Microglial activation and peripheral immune infiltration were cross-validated by flow cytometry, Western blotting, and immunohistochemistry. $^{89}$Zr-T2BA showed selective uptake in TREM2 OE cells and clearly distinguished WT from KO mice. Importantly, $^{89}$Zr-T2BA detects LPS-induced neuroinflammation without confounding peripheral immune infiltration. These findings position TREM2-targeted ImmunoPET as a promising microglia-specific imaging strategy to detect the inflammatory response in the brain.


# INTRODUCTION

Neuroinflammation is a complex inflammatory response to pathogens, misfolded proteins, and other tissue-damaging events [1,2]. It is an increasingly recognized central process in maintaining CNS homeostasis and a key component in the pathology of numerous neurological diseases when dysregulated [1,3]. Inflammation in the CNS can be a powerful tool in the defense against certain infections or injuries [4]. However, when neuroinflammation becomes chronic, its effects can cause significant damage in the CNS, commonly seen in neurodegenerative disorders [5]. Traditionally, the brain has been viewed as an immune-privileged organ, as it is separated from the rest of the body by the blood-brain barrier (BBB) [6]. Increasing evidence indicates that the CNS and its cellular components are under continuous surveillance by, and actively interact with, the immune system [7]. Under physiological conditions, the BBB restricts the entry of peripheral immune cells and circulating molecules, thereby preserving the brain's specialized microenvironment [8]. However, when the BBB is disrupted by infection or injury, peripheral immune cells, along with cytokines, chemokines, and other inflammatory mediators, can infiltrate the brain, leading to an amplified local immune response driven by resident central nervous system cells [2,8]. In a typical acute inflammatory response in the CNS, resident cells like microglia and astrocytes become activated, and a cascade of signaling molecules is released to recruit additional immune cells, engage local repair mechanisms, and even modulate neuronal activity [3,9]. Although these acute responses are initially neuroprotective, chronic activation can lead to a state of prolonged production of inflammatory and cytotoxic molecules [9,10]. This chronic exposure damages neurons, disrupts synaptic functioning, and ultimately contributes to the pathogenesis of neurodegenerative and neurological disorders [5,10,11].

Microglia, a type of macrophage located in the CNS, are resident immune cells that have a key role in neuroinflammation and undergo distinct morphological changes in accordance with their physiological states [12–14]. Unlike peripheral macrophages, which are continuously replaced from bone marrow precursors, microglial populations are sustained throughout life by self-renewal [15,16]. In their resting state, also termed the homeostatic or surveillant state, microglia display a type of ramified morphology, characterized by small cell bodies with many thin, motile processes that continuously scan the neural parenchyma for signs of disruption [17]. In this state, microglia also contribute to synaptic pruning, debris clearance, and production of neurotrophic factors that support neuronal health and plasticity [18]. Microglia can also undergo a rapid transformation from a more homeostatic state to various activated states upon the detection of pathogen-associated molecular patterns (PAMPs) or damage-associated molecular patterns (DAMPs) [19,20]. Activated microglia secrete numerous inflammatory molecules, such as interleukin-1β (IL-1β), tumor necrosis factor-alpha (TNF-α), reactive oxygen species (ROS), and nitric oxide (NO), which help to destroy pathogens and clear damaging debris [20,21]. However, these secretions can create collateral damage to healthy neural tissue if produced in excess [22,23].

Triggering receptor expressed on myeloid cells 2 (TREM2), a transmembrane protein predominantly found on microglia within the CNS, is capable of binding a wide range of ligands, including phospholipids, apoptotic debris, protein aggregates, and anionic molecules [24–26]. Through these interactions, TREM2 enhances microglial phagocytic capacity, balances cytokine secretion, and detects damage signals [24]. Upon ligand-binding, TREM2 associates with DNAX-activation protein of 12 kDa (DAP12 or TYROBP) and forms a protein complex, leading to downstream signaling events to phosphorylate cytosolic immunoreceptor tyrosine-based activation motifs (ITAMs) and recruits spleen tyrosine kinase (SYK) [26–28]. These events promote microglial activation and can help shift them from a purely proinflammatory state to one that incorporates tissue repair, which is essential in combating neuroinflammation [22,23].

Recent advances in noninvasive imaging techniques have reshaped the study of neuroinflammation by enabling real-time visualization of molecular and cellular events central to disease pathology, such as microglial activation [29,30]. Positron Emission Tomography (PET) and Magnetic Resonance Imaging (MRI) are the two most widely used modalities for assessing neuroinflammatory processes [30,31]. The development of radiolabeled bispecific antibodies (BsAbs) for imaging CNS disorders marks a major advancement in neurodegenerative disease research. By targeting the transferrin receptor (TfR) to bypass the BBB, these BsAbs allow noninvasive detection of crucial biomarkers, including Aβ in Alzheimer's Disease (AD). Recent work shows that refining BsAb design, such as reducing molecular size and adjusting binding affinity to transcytosis receptors, can improve brain uptake and clearance, thereby enhancing imaging contrast [32].

Because TREM2 plays a multifaceted role in microglial regulation, it has become a promising target in modulating and observing neuroinflammation. This work aimed to detect neuroinflammation by ImmunoPET with a TREM2 BsAb carrying a TfR-targeting construct that enables BBB penetration [33]. The

TREM2-TfR-BsAb was labeled with the positron emitter zirconium-89 ($^{89}$Zr) to visualize TREM2-expressing cells. The $^{89}$Zr-TREM2-Tfr-BsAb ($^{89}$Zr-T2BA) was validated for its specificity for TREM2 in cellular models and in a murine model of neuroinflammation.

## METHODS

All solvents and reagents were purchased from commercial suppliers (e.g., Millipore Sigma; Fisher Scientific) unless otherwise noted and were used without further purification. The chelator 1-(4-isothiocyanatophenyl)-3-[6,17-dihydroxy-7,10,18,21-tetraoxo-27-(Nacetylhydroxylamino)- 6,11,17, 22-tetraazaheptaeicosine] thiourea (p-SCN-Bn-DFO) was purchased from Macrocyclics, Inc. Molecular grade DMSO (> 99.9%: Sigma, D8418) was used as chelator stock solution. Zeba spin desalting columns (7K MWCO, 0.5–2.0 mL) and Cytiva disposable PD10 desalting columns were purchased from Fisher Scientific. The concentration of the DFO-conjugated antibody stock solution was measured on a Thermo Nanodrop ND-1000 UV-Vis spectrophotometer. $^{89}$Zr was produced at Washington University in St. Louis (WUSTL), Mallinckrodt Institute of Radiology. Radiolabeling synthesis reactions were monitored using silica-gel impregnated glass-microfiber instant thin-layer chromatography paper (iTLC-SG, Agilent) and analyzed on a dual scan-RAM radio-TLC plate reader using Laura radio-TLC software (LabLogic Systems, Inc.). Radioactivity was measured using a CRC-55tR dose calibrator (Capintec). All animal experiments were performed under a UTHealth Houston or UT MD Anderson Cancer Center Institutional Animal Care and Use Committee-approved (IACUC) protocol (AWC-24-0017, PI: Pisaneschi and 962-RN04, PI: Ray), and proper and humane use of animals in research followed the institutional guidelines. At least n = 4 animals per group were used. No animal was excluded from the study. All authors complied with ARRIVE guidelines in the manuscript.

# TREM2 antibody conjugation

The TREM2 and control antibody were produced as described by Zhao et al [33]. A small 7 kDa MWCO zeba spin column (0.5 mL) was placed in an Eppendorf tube and centrifuged at 1.5G for 1 minute, and the collected liquid was discarded. 300 µL of 0.1M $Na_2CO_3$ was added to the column, which was then centrifuged at 1.5 g for 1 minute. The collected liquid was discarded, and the process was repeated twice more. Subsequently, the column was put in a new Eppendorf tube. 1 mg of TREM2 or IgG control antibody stock solution in 1X phosphate saline buffer (PBS) was added to the column, which was then centrifuged at 1.5 g for 2 minutes. The collected liquid pH was adjusted to 8.5–9.0 by adding aliquots of 0.1M $Na_2CO_3$. Then 3–4 equivalents of p-SCN-Bn-DFO (in DMSO stock solution, 5 mg/mL) were added to the antibody mixture, and the mixture was incubated at 37°C for 2 hours. 15 minutes before the end of incubation, a large 7 kDa MWCO zeba spin column (2 mL) was washed three times by adding 1 mL PBS 1X into the column, centrifuging at 1000 rcf for 2 minutes, and discarding the collected liquid. After the buffer exchange in the large tube, the antibody mixture was removed from incubation, and everything was transferred into the big column, which was centrifuged at 1000 rcf for 2 minutes. The concentration of the DFO-conjugated antibody was measured by a UV-vis Nanodrop spectrophotometer.

## Radiolabeling of TREM2-DFO or IgG-DFO with Zr

Aliquots of $^{89}Zr$ in 1M oxalic acid were diluted by adding 100 µL of PBS 1X. The solution was neutralized to pH 7 by adding 1.0 M $Na_2CO_3$ (pH = 11), and subsequently, TREM2-DFO or IgG-DFO was added to the solution. The reaction mixture was incubated at 37°C for 1 hour, and the tube was gently shaken every 20 minutes. After 1 hour, labeling was ≥ 99%, as assessed by radio-iTLC (50Mm EDTA mobile phase, pH 5) using a silica gel impregnated glass microfiber iTLC plate, where the radiolabeled antibody remained at the baseline, and the $^{89}Zr^{4+}$ ions and $^{89}Zr$-EDTA eluted with the solvent front. Size-exclusion chromatography using PD10 columns eluting with PBS 1X was performed for purification of the $^{89}Zr$-radiolabeled antibodies.

## Serum stability test of Zr-T2BA and Zr-IgG-TfR

Both TREM2 and IgG antibodies were analyzed for their serum stability in human and mouse serum. Human and mouse serum solutions were thawed at 4°C over 24 h in preparation for the experiment. In two Eppendorf tubes, 200 µL of human serum was added to each. In one tube, $^{89}Zr$-T2BA (3.7 MBq) was added; in the other, $^{89}Zr$-IgG-TfR (3.7 MBq) was added. The mixture was shaken gently by hand for a few seconds at room temperature. Radio-TLC of these two mixtures was performed at 1 h, 24 h, and 48 h. The same experimental procedure and time-point analysis were repeated with mouse serum.

## Cell Lines and Cell Studies

TREM2 overexpressing (OE) and wild-type (WT) HEK293T cell lines were purchased from Creative Biogen Biotechnology (Cat No:CSC-RO0889). Cells were maintained in RPMI-1640 media supplemented with L-glutamine (Cytiva Lifesciences, SH30027.LS), 10% fetal bovine serum (FBS) (Corning, MT35015CV), and 1% penicillin/streptomycin (Gibco, 15140122). Cells were cultured at 37°C in a humidified atmosphere with 5% $CO_2$. To maintain selection pressure, 1 µg/mL puromycin was added to the media specifically for the TREM2 OE HEK293T cells.

To measure antibody binding by flow cytometry, WT and TREM2 OE cells were incubated with a mouse Fc blocking reagent for 10 min on ice. Subsequently, cells were surface-stained with unlabeled T2BA or IgG-TfR for 1 h on ice. Bound antibodies were detected with an anti-mouse IgG secondary antibody (BioLegend). Cells were collected for analysis using a BD LSRFortessa, and data were analyzed using FlowJo.

For cellular uptake experiments of $^{89}Zr$-TB2A, cells were seeded in V-bottom 96-well plates at a density of 20,000 cells per well in FBS-free media. Cells were then incubated with approximately 0.7 MBq of $^{89}Zr$-labeled antibodies. After incubation for 30 and 60 minutes, cells were pelleted by centrifugation at 700 x g for 5 minutes. The supernatant containing the radioactive tracer was carefully aspirated. Cells were subsequently washed three times with PBS. Finally, cells were lysed using RIPA buffer supplemented

with protease inhibitors. Radioactivity in the cell lysates was measured using a gamma counter. After radiometric counting, the total protein concentration in each well was determined using the BCA assay, and cellular uptake results were normalized to protein micrograms [34].

## Western Blot Analysis

WT and TREM2 OE HEK293T cell lines were lysed with RIPA buffer containing protease inhibitors. Cellular protein extracts were obtained by centrifugation at 15,000 x g for 15 minutes at 4°C. Thirty micrograms (30 µg) of protein from each sample were separated by SDS-PAGE and subsequently transferred to PVDF membranes. After blocking, membranes were incubated overnight at 4°C with primary antibodies: mouse anti-TREM2 (R&D Systems, AF1729) or human anti-GAPDH (Proteintech, 10494-1-AP). Following incubation with appropriate secondary antibodies for one hour at room temperature, protein bands specific for TREM2 and GAPDH were visualized using enhanced chemiluminescence (ECL) detection. Densitometric analysis of the protein bands was performed using ImageJ software, and TREM2 levels were normalized to GAPDH levels for each sample.

Brain tissues were homogenized in ice-cold RIPA buffer (Thermo Fisher Scientific) supplemented with protease and phosphatase inhibitor cocktails (Roche) using a sonicator. Homogenates were incubated on ice for 30 min and centrifuged at 14,000 × g for 15 min at 4°C to remove debris. The supernatants were collected, and total protein concentrations were determined using the BCA Protein Assay Kit (Thermo Fisher Scientific). Equal amounts of protein (40 µg) were mixed with 4× Laemmli sample buffer containing β-mercaptoethanol, heated at 95°C for 5 min, and separated on 4–12% SDS-polyacrylamide gels (Invitrogen). Proteins were transferred to PVDF membranes (Millipore) using a semi-dry transfer system. Membranes were blocked with Intercept (TBS) Blocking Buffer (Licor Bio) for 1 h at room temperature and incubated overnight at 4°C with primary antibodies diluted in blocking buffer. After washing with TBST, membranes were incubated with IRDye-conjugated secondary antibodies for 1 h at room temperature. Protein bands were visualized with an Odyssey M Imaging System (Licor Bio) and normalized using GAPDH as a loading control.

**LPS Dosing, Brain Dissociation, and Flow Cytometry for ex vivo Cross-Validation**

Adult mice were administered LPS (Sigma-Aldrich, L4391; 2 mg/kg, intraperitoneally), and euthanized at 24 h or 48 h post-injection. Following deep anesthesia, animals were transcardially perfused with cold phosphate-buffered saline (PBS) to remove circulating blood cells. Whole brains were rapidly dissected and transferred into Hibernate-A medium (Thermo Fisher Scientific) on ice until processing.

Single-cell suspensions were generated using the Adult Mouse Brain Dissociation Kit (Miltenyi Biotec) according to the manufacturer's instructions. The resulting cell suspensions were filtered through a 70 µm cell strainer, washed, and resuspended in FACS buffer (1x MojoSort Buffer).

For flow cytometric analysis, single cells were first incubated with anti-mouse CD16/CD32 Fc-blocking antibody to prevent nonspecific binding, followed by surface staining with fluorochrome-conjugated antibodies against CD11b and CD45. Samples were acquired using a BD LSRFortessa, and data were analyzed using FlowJo software. CD45high cells were defined as infiltrating peripheral immune cells, whereas CD45lowCD11b$^{+}$ cells were gated as microglia.

# LPS Dosing, PET Imaging, and Analysis

Eight-week-old, male C57BL/6J mice (Jackson Lab, stock #: 000664) and TREM2 knockout (KO) mice (C57BL/6J-*Trem2*$^{em2Adiuj}$/J, Jackson Lab, stock #: 027197) were utilized. Mice were housed in a facility with a 12-hour light/dark cycle and had ad libitum access to food and water. To establish an inflammatory model, experimental animals received 2 mg/kg LPS (Sigma-Aldrich, L4391) administered intraperitoneally. LPS injections were administered 2 hours before and 24 hours after tracer injection [35]. Approximately 0.8 MBq of $^{89}$Zr-labeled antibodies were injected into the tail vein of anesthetized mice, two hours after the initial LPS injection. CT-PET scans were performed at 24- and 48-hours post-tracer injection.

Mice were briefly anesthetized (typically < 5 minutes) using 1–2% isoflurane with oxygen as a carrier gas. Animals received intravenous tail vein injections of either $^{89}$Zr-T2BA or $^{89}$Zr-IgG-TfR (isotype control) in sterile saline, targeting a dose of 0.7 MBq in a total volume of 150 µL per mouse. The actual injected dose was precisely determined by measuring the pre- and post-injection activity of the syringe using a dose calibrator (Capintec). After injection, mice were returned to their cages and allowed ad libitum access to food and water until the next day. For imaging, mice were re-anesthetized using 1–3% isoflurane and transferred to a preclinical PET/SPECT/CT system (Albira PET/SPECT/CT, Bruker). Anesthesia was maintained at 0.5-2% isoflurane with continuous respiratory monitoring throughout the acquisition. PET images were acquired for 10 minutes using a 15 cm field of view (FOV). Corresponding CT images were acquired for fusion using a 7 cm FOV. Images were reconstructed using the Maximum Likelihood Expectation Maximization (MLEM) algorithm for PET and the Filtered Back Projection (FBP) for CT, and then automatically fused by using PMOD 4.3 software (Pmod Technologies, Faellanden, Switzerland). Regional brain PET analyses were carried out by using the mouse brain atlas in the software. All data were decay-corrected and expressed as a percentage of injected dose per cubic centimeter (%ID/cc).

## Immunohistochemical Evaluations

After the last PET imaging (48 h), mice were sacrificed, and the brain tissues were harvested in a tissue cassette and preserved in 10% neutral buffered formalin (Azer Scientific) overnight. The tissues were then washed with PBS and kept in 70% ethanol until the analysis. Downstream tissue processing and IHC staining were conducted by HistoWiz. IBA1 (Catalog # 019-19741) and Ly6C/Ly6G (Catalog #

ab25377) antibodies were selected to detect activated microglial cells and discriminate the peripheral leukocytes, respectively.

# Statistical Analysis

All statistical analyses were conducted using GraphPad Prism 10 software (Version 10.1.2). ANOVA test was used to compare multiple *in vitro* groups. The Mann–Whitney U test was used for comparisons between two independent groups, while the Kruskal–Wallis test and then the Dunn—Bonferroni test was applied for comparisons involving more than two independent groups for the animal studies.

## RESULTS

# Radiochemistry

To confirm antibody specificity and binding before labeling, TREM2 OE cells and parental controls were surface-stained with increasing doses of unlabeled T2BA or IgG-TfR. Western blot analysis was first performed on both cell lines to confirm TREM2 overexpression; as expected, TREM2 expression was not observed in the parent cell line. In contrast, high TREM2 protein expression was detected in the TREM2 OE cell line **(Supplemental Fig. 1A & B)**. Accordingly, flow cytometry analysis showed that T2BA binding was detected only in TREM2 OE cells (Fig. 1A). After radiolabeling, the activity yields of $^{89}$Zr-T2BA and $^{89}$Zr-IgG-TfR control were 74 ± 3% (n = 6) and 76 ± 3% (n = 6), respectively. Both antibodies had radiochemical purity greater than 99% (Fig. 1B), and the labeled antibodies were stable in PBS at 4°C for up to 48 hours. The specific activities of $^{89}$Zr-T2BA and $^{89}$Zr-IgG-TfR were calculated as 0.54 MBq/μg and 0.44 MBq/μg, respectively. Both antibodies remained stable in human and mouse serum up to 48 h, as determined by radio-TLC analysis.

**Validation in vitro and in vivo**

TREM2 OE and WT HEK293T cells were also used to investigate the cellular uptake of $^{89}$Zr-T2BA *in vitro* **(**Fig. 1C**)**. Cells were incubated with $^{89}$Zr-T2BA or $^{89}$Zr-IgG-TfR for 30 or 60 min. $^{89}$Zr-T2BA bound to the TREM2 OE cell line at more than two-fold higher levels than WT cells at both time points (30 and 60 minutes). Compared to $^{89}$Zr-IgG-TfR, $^{89}$Zr-T2BA retention was 11.1- and 10.3-fold higher on TREM2 OE and 1.5- and 1.8-fold higher in WT cells after 30 and 60 minutes of incubation, respectively (Fig. 1C).

Healthy WT and TREM2 KO mice were used to demonstrate the *in vivo* TREM2 specificity of $^{89}$Zr-T2BA. PET images were acquired at 24 and 48 h post-injection of the tracer. The lowest brain uptake of $^{89}$Zr-T2BA was observed in the healthy TREM2 KO mice, as expected (Fig. 2A-B). WT mice showed more than a five-fold higher brain uptake of $^{89}$Zr-T2BA compared to TREM2 KO mice. In healthy WT mice, no statistically significant differences were observed in brain uptake of $^{89}$Zr-T2BA or $^{89}$Zr-IgG-TfR, suggesting that the probe cannot differentiate basal TREM2 expression at this time point when compared to the isotype control.

Using LPS to induce neuroinflammation, $^{89}$Zr-T2BA activity was tested on WT and TREM2 KO mice. Under inflammatory conditions, WT mice showed a two-fold, statistically significant higher $^{89}$Zr-T2BA brain uptake when compared to the isotype control (4.49%ID/cc vs. 3.20%ID/cc) and a six-fold higher uptake (4.49%ID/cc vs. 0.82%ID/cc) compared to the inflamed brains of TREM2 KO animals (Fig. 2C-D). Finally, $^{89}$Zr-T2BA uptake was two-fold higher in the brain of LPS-inflamed versus healthy animals (4.49%ID/cc vs. 3.24%ID/cc) (Fig. 2A **& C**, orange bars). As expected, LPS-induced inflammatory conditions in TREM2 KO mice did not cause a significant increase in brain uptake of $^{89}$Zr-T2BA (Fig. 2C). Regional brain PET analysis showed that LPS-treated mice had statistically significantly higher uptake across the whole brain averages and also in specific regions, like the hippocampus (0.521 SUV vs. 0.376 SUV), thalamus (0.573 SUV vs. 0.398 SUV), cortex (0.461 SUV vs. 0.371 SUV), cerebellum (0.542 SUV vs. 0.440 SUV), and striatum (0.508 SUV vs. 0.365) compared with WT control mice (Fig. 2E-F).

All body PET and biodistribution patterns were analyzed in healthy and LPS-inflamed WT animals after 48h of the injection of $^{89}$Zr-T2BA and the isotope control (Fig. 3A **& B, Supplemental Fig. 3**). Organs with the highest activity were found to be the liver, kidney, bone, and spleen (Fig. 3A). Uptake in the kidney and liver appears to be partially TREM2-mediated, but independent of inflammation status, whereas in the spleen, the highest uptake is, as expected, with $^{89}$Zr-T2BA in LPS-inflamed animals. Bone uptake was also unusually higher, likely as a result of TREM2 being expressed in osteoclasts [36,37].

All body PET and biodistribution patterns were also analyzed in healthy and LPS-inflamed TREM2 KO animals after 48h of the injection of $^{89}$Zr-T2BA and the isotope control, $^{89}$Zr-IgG-TfR (**Supplemental Fig. 2A & B, and 4**). Similar to the WT cohort, the organ which had the highest activity were found to be the liver, kidney, and spleen (**Supplemental Fig. 2A**) with lower uptake in bone compared to WT animals (Fig. 3A).

**Cross-validation ex vivo**

Flow cytometry analyses revealed a lack of peripheral immune infiltration accompanied by significant microglial activation in the brains of LPS-administered mice (Fig. 4, A**&B**). Moreover, increased IBA1 levels, an indicator of microgliosis, were detected by Western blot and IHC in LPS-treated mice (Fig. 4C). IBA1 IHC analyses demonstrated that microglia in LPS-treated mice exhibited enlarged cell bodies and increased branching complexity, consistent with an activated microglial phenotype (Fig. 4C; **arrows**). Accordingly, these microglia showed increased CD45 surface levels and higher granularity (Fig. 4D). Ly6C/Ly6G-positive cells were not detected in the brain sections of LPS-dosed or control mice (Fig. 4C), confirming the absence of peripheral immune infiltration observed by flow cytometry.

# DISCUSSION

In this study, a novel tracer targeting TREM2, $^{89}$Zr-T2BA, was developed and evaluated for noninvasive visualization of neuroinflammatory responses linked to TREM2-mediated microglial activation. The tracer is based on a bispecific antibody engineered to target TREM2 and the transferrin receptor, the

latter enabling BBB penetration. $^{89}$Zr-T2BA was produced in high yields and radiochemical purity. When testing for TREM2 specificity in cell culture, $^{89}$Zr-T2BA displayed higher uptake in HEK293T cells engineered to overexpress TREM2 than in WT, parental HEK293T cells, and uptake of the isotype control antibody in both cell lines. This is a clear indication that $^{89}$Zr-T2BA binds to TREM2 in this cellular model. *In vivo*, $^{89}$Zr-T2BA was tested in WT and TREM2 KO animals. Uptake of $^{89}$Zr-T2BA in the brain of WT animals trended higher at 48 h post-injection of the tracer, even if statistical significance was not reached. This suggests that the probe cannot differentiate basal TREM2 expression. Interestingly, in TREM2 KO mice, $^{89}$Zr-T2BA showed reduced uptake compared to $^{89}$Zr-IgG-TfR, indicating very low Fc receptor-mediated binding of $^{89}$Zr-T2BA *in vivo*, and further supporting its ability to exclusively detect TREM2-expressing cells.

In TREM2 KO animals, $^{89}$Zr-T2BA uptake was 5.4-fold lower, confirming the probe's *in vivo* TREM2 specificity, as previously observed in cells. In LPS-treated WT animals, $^{89}$Zr-T2BA showed robust accumulation in brain regions at both 24- and 48-hours post-injection relative to isotype control. Notably, this signal was markedly reduced in TREM2 KO animals, supporting target-specific binding. Given that TREM2 expression within the CNS is largely restricted to microglia, these findings are consistent with increased tracer uptake driven by microglial activation and expansion during neuroinflammation.

Complementary cellular and immunohistochemical analyses confirmed pronounced microglial population and activation in response to LPS with minimal infiltration of peripheral immune cells into the brain. Together, these data indicate that the PET signal predominantly reflects microglial TREM2 expression rather than contributions from peripheral myeloid populations [38,39]. While TREM2 is also expressed by macrophages and other innate immune cells in the periphery, the limited immune cell infiltration into the CNS in this model supports the interpretation that brain tracer uptake primarily represents microglia-associated neuroinflammatory activity.

Two examples of TREM2-PET have been reported in the literature while this work was in progress. Shojaei et al. reported a copper-64 labeled, TREM2-targeting 4D9 antibody PET tracer evaluated it and a control without an ATV in AD mouse models to image TREM2 expression *in vivo*. By conjugating the 4D9 anti-TREM2 antibody to a NODAGA chelator, with or without an antibody transport vehicle to enhance BBB crossing, they demonstrated increased cortical and hippocampal tracer uptake in 5xFAD;TfR$^{mu/hu}$ mice compared with wild-type controls that were without a human TfR binding agent, findings that were confirmed by *ex vivo* autoradiography [40]. More recently, Dahlén et al. engineered and compared three bispecific anti-TREM2 antibodies incorporating different TfR binders to enhance BBB transcytosis. They quantified blood pharmacokinetics and *ex vivo* brain uptake in AppNL-G-F transgenic and wild-type mice using $^{125}$I labeling and γ-counting up to 72 h post-injection. Among the constructs, the IgG-scFv$_2$ format - containing two scFv8D3 TfR binders - achieved the highest brain concentrations and accumulated significantly more in AppNL-G-F brains than in wild-type mice at both 48 and 72 hours. When this lead construct was labeled with $^{124}$I for *in vivo* PET imaging, it enabled visualization and quantification of increased TREM2 signal in AppNL-G-F mice by PET, with TREM2 concentration measured in the brains *ex*

*vivo* [41]. Although the animal models and radiotracers used in this study differ from those previously reported, regional brain PET analyses revealed a similar pattern of tracer uptake. Specifically, $^{89}$Zr-T2BA showed higher uptake in the hippocampus, thalamus, cortex, cerebellum, and striatum, in LPS-treated mice compared with wild-type controls. Importantly, our results further demonstrate that the TfR-binding region effectively facilitates tracer delivery across the BBB into the brain.

TREM2 is one of the newest markers of neuroinflammation emerging in the imaging field, but imaging of neuroinflammation has been an active field of investigation for many years, with the most notable efforts focused on visualizing the translocator protein (TSPO). TSPO is not exclusively expressed by microglia in the brain; it is also found in astrocytes, vascular endothelial cells, and certain neurons [42]. In addition, some human postmortem studies of AD brains have failed to show meaningful elevations in TSPO, demonstrating a limitation of TSPO-PET for imaging neuroinflammation in neurodegenerative conditions [43]. State-of-the-art PET tracers used to assess neuroinflammation still largely target TSPO, spanning first-, second-, and third-generation radioligands, but all face major limitations, including stronger signals in rodents than in humans, substantial genetic polymorphism effects, and high levels of nonspecific binding. [44–46]. Consequently, there is a pressing need for novel PET tracers with greater specificity to enable noninvasive diagnosis and risk assessment in neuroinflammation research. Other molecular targets could enable more specific characterization of microglial states, ranging from homeostatic to proinflammatory phenotypes. Among these, Colony-stimulating factor 1 receptor (CSF1R) is a cell surface receptor that plays a crucial role in the survival, proliferation, and differentiation of myeloid cells. CSF1R levels are significantly elevated in diseases associated with marked neuroinflammation, such as AD, multiple sclerosis, and glioblastomas [47]. The very first attempt to develop a CSF1R-specific PET tracer, namely $^{11}$C-AZ683, was hampered by low BBB penetration in rodents and non-human primates [48]. More research, conducted by Horti et al., uses a new CSF1R targeted radiotracer, $^{11}$C-CPPC. Although $^{11}$C-CPPC has shown promising results in models of LPS-induced neuroinflammation and experimental autoimmune encephalomyelitis *in vivo* and even in human AD brain tissues, higher nonspecific binding remains a problem to be addressed [49]. PET tracers targeting the P2X ligand-gated ion channel type 7 receptor (P2X7R), which is an ionotropic receptor activated by ATP and implicated in microglial proliferation, activation, and apoptosis, have shown limitations, including low CNS uptake and limited lack of specificity due to high intersubject variability [50]. There is only one tracer, namely $^{11}$C-SMW139, which has progressed to human pharmacokinetic studies and has shown increased *in vivo* binding potential in patients with relapsing remitting MS compared with age-matched healthy controls [51]. $^{11}$C-SMW139 was recently assessed in a multicenter study and showed higher uptake in PD patients [52]. Purinergic metabotropic 12 receptor (P2Y12R) is a chemoreceptor for adenosine diphosphate expressed peripherally on platelets but localized primarily to microglia within the CNS [53]. A $^{11}$C-labelled PET tracer targeting P2Y12R showed strong affinity to P2Y12R, but low BBB penetrance [54]. Beyond receptor-targeted approaches, metabolic imaging of neuroinflammation has also been explored. A recent study displayed that LPS-inflamed brain tissue takes up significantly more fructose than healthy tissue, and

that a novel radiotracer, 4-[$^{18}$F]FDF, can detect this difference via PET imaging with low background signal in healthy brains [55].

There remains an unmet need for novel molecular targets and radiotracers to better characterize neuroinflammation in CNS disorders. The data presented here demonstrate that $^{89}$Zr-T2BA exhibits higher target-to-background ratios and prolonged signal retention in inflamed tissue, consistent with stable and specific target engagement. Collectively, these findings support further development of this tracer as a promising candidate to address this unmet need.

## Declarations

# Competing Interests

The UTHealth Houston Office of Technology has filed a patent application for novel TREM2-specific antibodies, naming Z.A. and N.Z. as inventors. F.P. is an Associate Editor of npj Imaging. She was not involved in the handling or editorial decision-making process of this manuscript. The remaining authors declare no competing interests.

# Author Contribution

Specific author contributions are as follows: conception and design of experiments by E.K, O.O., T.M.B., Y.L.L, W.J.R. and F.P.; antibody production and quality control by W.X., Z.A., and N.Z.; experimental and data acquisition by E.K., O.O., T.M.B, R.P.T, W.X.; analysis and interpretation of the data by E.K, O.O, T.M.B., Y.L.L, and F.P.;  E.K, O.O, T.M.B., Y.L.L, and F.P. wrote the main manuscript text and prepared figures. All authors contributed to the revision of the manuscript and approved the final content. E.K and O.O. contributed equally.

# Acknowledgement

The author would like to thank the small animal imaging facility (SAIF) at UT MD Anderson Cancer Center, and the staff members therein, in particular Charles Kingsley, Emily Newsom, Jennifer Meyer, Mark Cabrera, and Xavier Sauceda. The SAIF is supported by the NIH-NCI Cancer Center Support Grant CA016672 (G. Draetta). This work was supported by UT Health internal resources (F.P.), and partially supported by the Welch Foundation (AU-0042-20030616 to Z.A.) and the Lindonlight Collective (GR-25-004 to Z.A.).

# Data Availability

Data is available upon reasonable request to the corresponding author.

# References


1. Ahmad, M. A. *et al.* Neuroinflammation: A Potential Risk for Dementia. *Int. J. Mol. Sci.* 23, 616 (2022-01-06). https://doi.org/10.3390/ijms23020616
2. Kölliker-Frers, R. *et al.* Neuroinflammation: An Integrating Overview of Reactive-Neuroimmune Cell Interactions in Health and Disease. *Mediators Inflamm.* 2021, 1–20 (2021). https://doi.org/10.1155/2021/9999146
3. Müller, L. *et al.* From Homeostasis to Neuroinflammation: Insights into Cellular and Molecular Interactions and Network Dynamics. *Cells* 14, 54 (2025-01-05). https://doi.org/10.3390/cells14010054
4. Zhang, W. *et al.* Role of neuroinflammation in neurodegeneration development. *Signal Transduct. Target. Ther.* 8 (2023-07-12). https://doi.org/10.1038/s41392-023-01486-5
5. Adamu, A., Li, S., Gao, F. & Xue, G. Frontiers | The role of neuroinflammation in neurodegenerative diseases: current understanding and future therapeutic targets. *Front. Aging Neurosci.* 16 (2024/04/12). https://doi.org/10.3389/fnagi.2024.1347987
6. Cervellati, C., Trentini, A., Pecorelli, A. & Valacchi, G. Inflammation in Neurological Disorders: The Thin Boundary Between Brain and Periphery. *Antioxid. Redox Signal* 33 (2020-06–18). https://doi.org/10.1089/ars.2020.8076
7. Streit, W. J. & Kincaid-Colton, C. A. The Brain's Immune System. *Sci. Am.* 273, 54–61 (1995).
8. Müller, L. & Di Benedetto, S. Frontiers | Neuroimmune crosstalk in chronic neuroinflammation: microglial interactions and immune modulation. *Front. Cell. Neurosci.* 19 (2025/04/07). https://doi.org/10.3389/fncel.2025.1575022
9. Shabab, T., Khanabdali, R., Moghadamtousi, S. Z., Kadir, H. A. & Mohan, G. Neuroinflammation pathways: a general review. *Int. J. Neurosci.* 127 (2017-7-3). https://doi.org/10.1080/00207454.2016.1212854
10. Lyman, M., Lloyd, D. G., Ji, X., Vizcaychipi, M. P. & Ma, D. Neuroinflammation: The role and consequences. *Neurosci. Res.* 79 (2014/02/01). https://doi.org/10.1016/j.neures.2013.10.004
11. CK, G., K, S., B, W., MC, M. & FH, G. Mechanisms underlying inflammation in neurodegeneration - PubMed. *Cell* 140 (03/19/2010). https://doi.org/10.1016/j.cell.2010.02.016
12. Marshall, J. S. *et al.* An introduction to immunology and immunopathology. *Allergy Asthma Clin. Immunol.* 14 (2018-09-12). https://doi.org/10.1186/s13223-018-0278-1
13. Martins-Ferreira, R. *et al.* The Human Microglia Atlas (HuMicA) unravels changes in disease-associated microglia subsets across neurodegenerative conditions. *Nat. Commun.* 16 (2025). https://doi.org/10.1038/s41467-025-56124-1
14. Shimizu, T. & Prinz, M. Microglia across evolution: from conserved origins to functional divergence. *Cell. Mol. Immunol.* 22, 1533–1548 (2025). https://doi.org/10.1038/s41423-025-01368-6
15. Kabba, J. A. *et al.* Microglia: Housekeeper of the Central Nervous System. *Cell. Mol. Neurobiol.* 38 (2017-05-22). https://doi.org/10.1007/s10571-017-0504-2

16. Rossi, F., Lewis, C., Rossi, F. & Lewis, C. Microglia's heretical self-renewal. *Nat. Neurosci.* 21 (2018-03–28). https://doi.org/10.1038/s41593-018-0123-3
17. Bachiller, S. *et al.* Frontiers | Microglia in Neurological Diseases: A Road Map to Brain-Disease Dependent-Inflammatory Response. *Front. Cell. Neurosci.* 12 (2018/12/18). https://doi.org/10.3389/fncel.2018.00488
18. Gao, C. *et al.* Microglia in neurodegenerative diseases: mechanism and potential therapeutic targets. *Signal Transduct. Target. Ther.* 8 (2023-09-22). https://doi.org/10.1038/s41392-023-01588-0
19. Santoni, G. *et al.* Danger- and pathogen-associated molecular patterns recognition by pattern-recognition receptors and ion channels of the transient receptor potential family triggers the inflammasome activation in immune cells and sensory neurons. *J. Immunol.* 12 (2015-02–03). https://doi.org/10.1186/s12974-015-0239-2
20. Fiebich, B. L., Batista, C. R. A., Saliba, S. W., Yousif, N. M. & de Oliveira, A. C. P. Frontiers | Role of Microglia TLRs in Neurodegeneration. *Front. Cell. Neurosci.* 12 (2018/10/02). https://doi.org/10.3389/fncel.2018.00329
21. Simpson, D. S. A., Oliver, P. L., Simpson, D. S. A. & Oliver, P. L. ROS Generation in Microglia: Understanding Oxidative Stress and Inflammation in Neurodegenerative Disease. *Antioxid. Redox Signal* 9, 743 (2020-08-13). https://doi.org/10.3390/antiox9080743
22. Fu, W.-Y., Wang, X. & Ip, N. Y. Targeting Neuroinflammation as a Therapeutic Strategy for Alzheimer's Disease: Mechanisms, Drug Candidates, and New Opportunities. *ACS Chem. Neurosci.* (September 17, 2018). https://doi.org/10.1021/acschemneuro.8b00402
23. Predonzani, A., Cal&igrave, B., Agnellini, A. H. & Molon, B. Spotlights on immunological effects of reactive nitrogen species: When inflammation says nitric oxide. *http://www.wjgnet.com/* 5 (May 20, 2015). https://doi.org/10.5493/wjem.v5.i2.64
24. Boyd, R. J. *et al.* Neuroinflammation represents a common theme amongst genetic and environmental risk factors for Alzheimer and Parkinson diseases. *J. Immunol.* 19 (2022-09–08). https://doi.org/10.1186/s12974-022-02584-x
25. MR, D. *et al.* Pattern recognition by TREM-2: binding of anionic ligands - PubMed. *J. Immunol.* 171 (07/15/2003). https://doi.org/10.4049/jimmunol.171.2.594
26. Colonna, M. & Colonna, M. The biology of TREM receptors. *Nat. Rev. Immunol.* 23 (2023-02-07). https://doi.org/10.1038/s41577-023-00837-1
27. Yao, H. *et al.* Frontiers | Distinct Signaling Pathways Regulate TREM2 Phagocytic and NFκB Antagonistic Activities. *Front. Cell. Neurosci.* 13 (2019/10/10). https://doi.org/10.3389/fncel.2019.00457
28. Ford, J. W. & McVicar, D. W. TREM and TREM-like receptors in inflammation and disease. *Curr. Opin. Immunol.* 21 (2009/02/01). https://doi.org/10.1016/j.coi.2009.01.009
29. Hammoud, D. A. Molecular Imaging of Inflammation: Current Status. *J. Nucl. Med.* 57 (2016-08–01). https://doi.org/10.2967/jnumed.115.161182

30. Aiello, M. *et al.* Neuroinflammation in Neurodegenerative Diseases: Current Multi-modal Imaging Studies and Future Opportunities for Hybrid PET/MRI. *J. Neurosci.* 403 (2019/04/01). https://doi.org/10.1016/j.neuroscience.2018.07.033
31. Gotthardt, M., Bleeker-Rovers, C. P., Boerman, O. C. & Oyen, W. J. G. Imaging of Inflammation by PET, Conventional Scintigraphy, and Other Imaging Techniques. *J. Nucl. Med.* 51 (2010-12–01). https://doi.org/10.2967/jnumed.110.076232
32. Roohani, B., Mendez, A. S., Dangarwala, M., Katz, S. & Marquez-Nostra, B. Nuclear Imaging of Bispecific Antibodies on the Rise. *J Nucl Med* 65, 1512–1517 (2024). https://doi.org/10.2967/jnumed.123.267215
33. Zhao, P. *et al.* Discovery and engineering of an anti-TREM2 antibody to promote amyloid plaque clearance by microglia in 5XFAD mice. *mAbs* 14 (2022-12-31). https://doi.org/10.1080/19420862.2022.2107971
34. Witney, T. H. *et al.* Preclinical Evaluation of 3-18F-Fluoro-2,2-Dimethylpropionic Acid as an Imaging Agent for Tumor Detection. *J. Nucl. Med.* 55 (2014-09-01). https://doi.org/10.2967/jnumed.114.140343
35. Kim, J. *et al.* Repeated LPS induces training and tolerance of microglial responses across brain regions. *J. Neuroinflammation* 21 (2024-09-20). https://doi.org/10.1186/s12974-024-03198-1
36. Abou, D. S., Ku, T. & Smith-Jones, P. M. In vivo biodistribution and accumulation of 89Zr in mice. *Nucl. Med. Biol.* 38, 675–681 (2011). https://doi.org/10.1016/j.nucmedbio.2010.12.011
37. Colonna, M. TREMs in the immune system and beyond. *Nat. Rev. Immunol.* 3, 445–453 (2003). https://doi.org/10.1038/nri1106
38. Konishi, H. & Kiyama, H. Microglial TREM2/DAP12 Signaling: A Double-Edged Sword in Neural Diseases. *Front. Cell. Neurosci.* 12 (2018). https://doi.org/10.3389/fncel.2018.00206
39. Shastri, A., Bonifati, D. M. & Kishore, U. Innate Immunity and Neuroinflammation. *Mediators Inflamm.* 2013, 1–19 (2013). https://doi.org/10.1155/2013/342931
40. Shojaei, M. *et al.* PET imaging of microglia in Alzheimer's disease using copper-64 labeled TREM2 antibodies. *Theranostics* 14, 6319–6336 (2024). https://doi.org/10.7150/thno.97149
41. Dahlen, A. D. *et al.* PET imaging of TREM2 in amyloid-beta induced neuroinflammation. *Eur. J. Nucl. Med. Mo.l Imaging* 52, 4320–4333 (2025). https://doi.org/10.1007/s00259-025-07358-0
42. Guilarte, T. R., Rodichkin, A. N., McGlothan, J. L., Rocha, A. M. A. D. L. & Azzam, D. J. Imaging neuroinflammation with TSPO: A new perspective on the cellular sources and subcellular localization. *Pharmacol. Ther.* 234 (2022/06/01). https://doi.org/10.1016/j.pharmthera.2021.108048
43. Masdeu, J. C., Pascual, B. & Fujita, M. Imaging Neuroinflammation in Neurodegenerative Disorders. *J. Nucl. Med.* 63, 45S-52S (2022). https://doi.org/10.2967/jnumed.121.263200
44. Uzuegbunam, B. C., Rummel, C., Librizzi, D., Culmsee, C. & Yousefı, B. H. Radiotracers for Imaging of Inflammatory Biomarkers TSPO and COX-2 in the Brain and in the Periphery. *Int. J. Mol. Sci.* 24 (2023 Dec 13). https://doi.org/10.3390/ijms242417419

45. Dahlén, A. D. *et al.* PET imaging of TREM2 in amyloid-beta induced neuroinflammation. *Eur. J. Nucl. Med. Mol. Imaging* 52 (2025-05-28). https://doi.org/10.1007/s00259-025-07358-0
46. Viviano, M. *et al.* Essential Principles and Recent Progress in the Development of TSPO PET Ligands for Neuroinflammation Imaging. *Curr. Med. Chem.* 29 (2022). https://doi.org/10.2174/0929867329666220329204054
47. Chitu, V., Gokhan, S., Nandi, S., Mehler, M. F. & Stanley, E. R. Emerging Roles for CSF-1 Receptor and its Ligands in the Nervous System. *Trends Neurosci.* 39, 378–393 (2016). https://doi.org/10.1016/j.tins.2016.03.005
48. Tanzey, S. S. *et al.* Synthesis and Initial In Vivo Evaluation of [(11)C]AZ683-A Novel PET Radiotracer for Colony Stimulating Factor 1 Receptor (CSF1R). *Pharmaceuticals (Basel)* 11 (2018). https://doi.org/10.3390/ph11040136
49. Horti, A. G. *et al.* PET imaging of microglia by targeting macrophage colony-stimulating factor 1 receptor (CSF1R). *Proc. Natl. Acad. Sci. U S A* 116, 1686–1691 (2019). https://doi.org/10.1073/pnas.1812155116
50. Jain, P. *et al.* Neuroinflammation PET Imaging: Current Opinion and Future Directions. *J. Nucl. Med.* 61, 1107–1112 (2020). https://doi.org/10.2967/jnumed.119.229443
51. Hagens, M. H. J. *et al.* The P2X(7) receptor tracer [(11)C]SMW139 as an in vivo marker of neuroinflammation in multiple sclerosis: a first-in man study. *Eur. J. Nucl. Med. Mol. Imaging* 47, 379–389 (2020). https://doi.org/10.1007/s00259-019-04550-x
52. Rikken, R. M. *et al.* Imaging Proinflammatory Microglia in Parkinson Disease Using [(11)C]SMW139 PET: A Multicenter Study. *J. Nucl. Med.* 66, 1646–1651 (2025). https://doi.org/10.2967/jnumed.125.269671
53. Beaino, W. *et al.* Purinergic receptors P2Y12R and P2X7R: potential targets for PET imaging of microglia phenotypes in multiple sclerosis. *J. Neuroinflammation* 14, 259 (2017). https://doi.org/10.1186/s12974-017-1034-z
54. Villa, A. *et al.* Identification of new molecular targets for PET imaging of the microglial anti-inflammatory activation state. *Theranostics* 8, 5400–5418 (2018). https://doi.org/10.7150/thno.25572
55. Kirby, A. *et al.* It's a Trap! Aldolase-Prescribed C < sub>4Deoxyradiofluorination Affords Intracellular Trapping and the Tracing of Fructose Metabolism by PET. *J. Nucl. Med.* 65, 475–480 (2024). https://doi.org/10.2967/jnumed.123.266905

# Figures

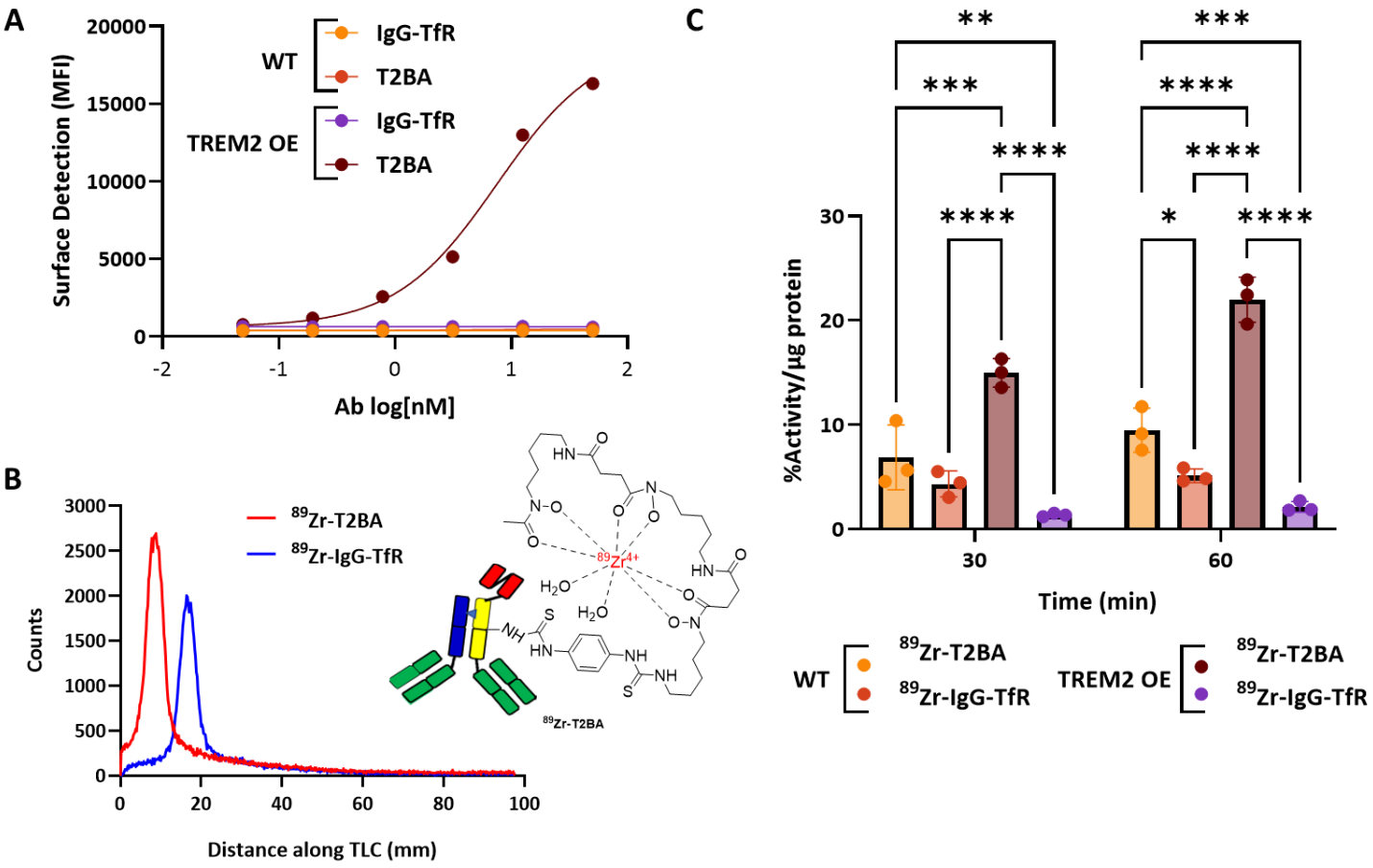


## Figure 1

**Chemical aspects and *in vitro* analyses** A) Binding affinity assay B) Radio TLC chromatogram of $^{89}$Zr-T2BA and $^{89}$Zr-IgG-TfR on iTLC-SG chromatography paper with 50 mM EDTA solution as eluent and schematic of chemical makeup. C) Cellular uptake results for $^{89}$Zr-T2BA and $^{89}$Zr-IgG-TfR after 30 minutes and 60 minutes incubation. In the bispecific antibody representation, green represents the mouse TREM2-binding moiety, yellow and blue represent the human IgG Fc-fragment (with mutations of knob/hole), and red represents single chain variable fragment (scFv) binding to transferrin receptor. C) Cellular uptake results for $^{89}$Zr-T2BA and $^{89}$Zr-IgG-TfR after 30 minutes and 60 minutes incubation.

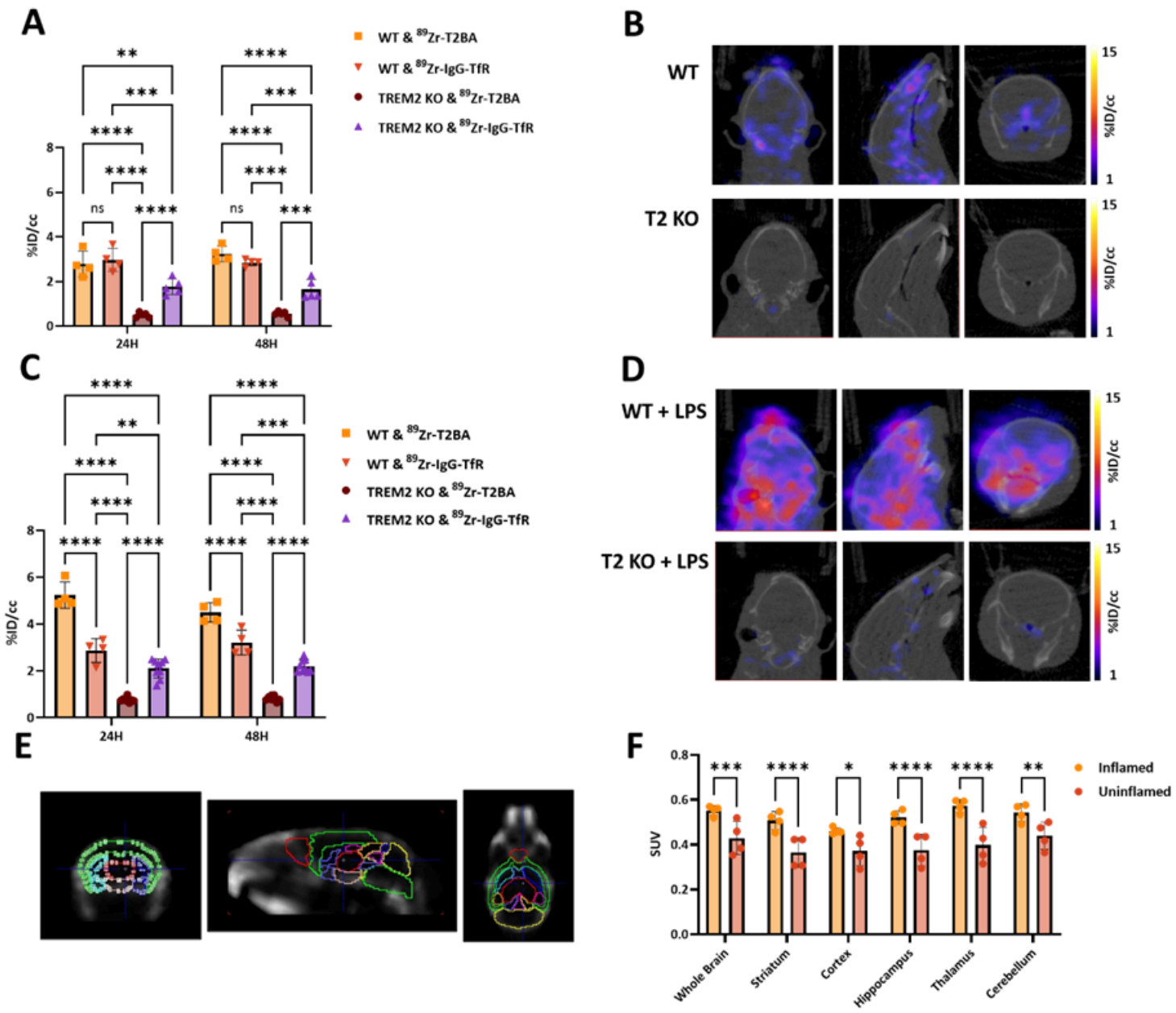


## Figure 2

**$^{89}$Zr-T2BA can detect TREM2 activation in an LPS-induced neuroinflammation model. *In vivo* specificity of $^{89}$Zr-T2BA**. A) Brain uptake of both Zr-labeled antibodies in healthy WT and TREM2 KO mice evaluated by PET analysis. B) Brain PET images of WT and TREM2 KO mice in healthy conditions (a: transverse, b: sagittal, c: coronal). C) Whole brain PET analysis for both Zr-labeled antibodies in WT and TREM2 KO LPS-inflamed mice. D) Brain PET images of $^{89}$Zr-T2BA signal in WT and TREM2 LPS-inflamed mice (a: transverse, b: sagittal, c: coronal). E) Comparative regional brain analysis setup. F) Uptake of $^{89}$Zr-T2BA in WT LPS-inflamed and uninflamed mice (whole brain values in this graph represent the average uptake of all regions).

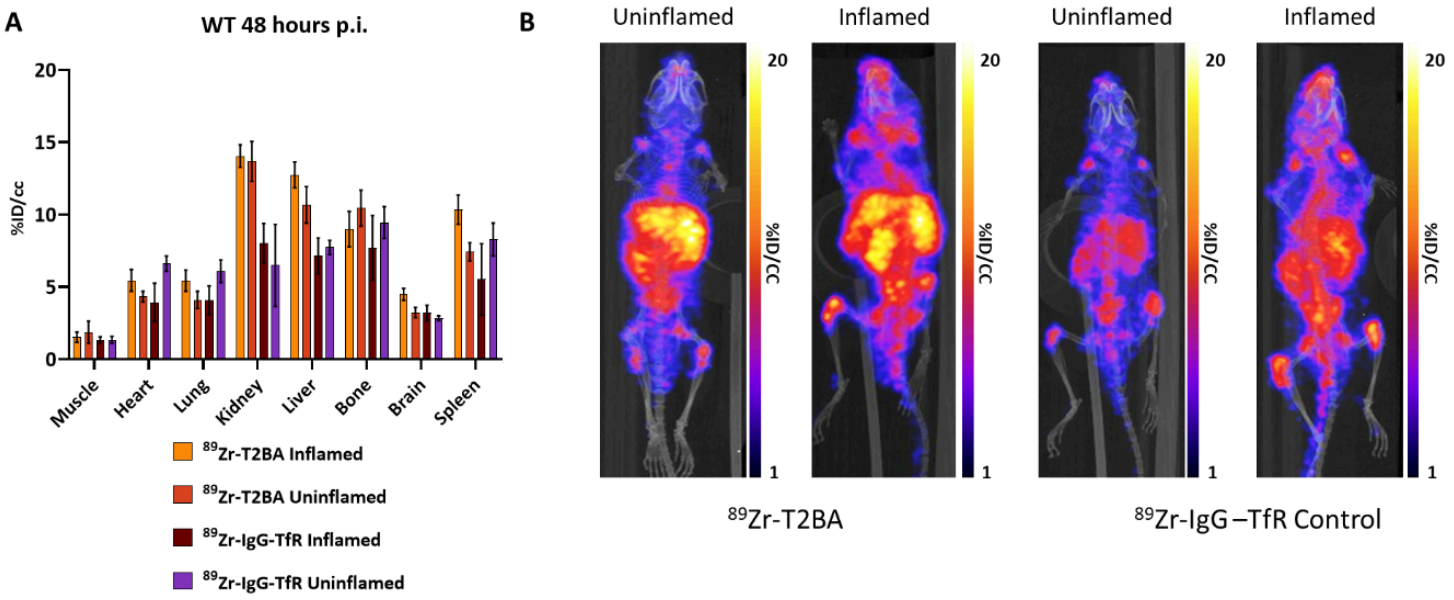


Figure 3

**$^{89}$Zr-T2BA biodistribution across conditions.** A) Uptake by organ in WT LPS-inflamed and uninflamed mice at 48 hours p.i. B) Whole body maximum intensity projection (MIP) PET images of WT LPS-inflamed and uninflamed mice at 48 hours p.i.

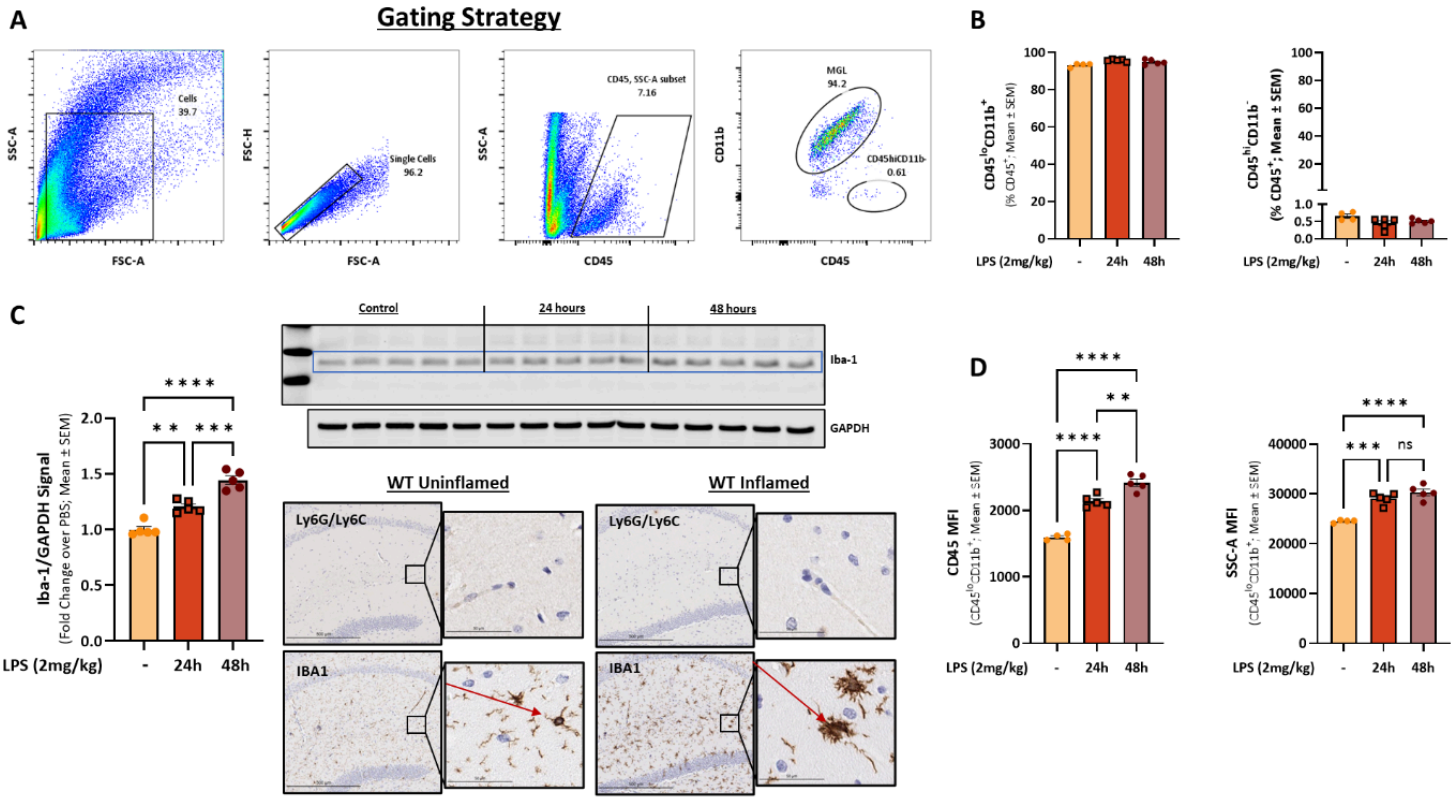


Figure 4

**PET signal is predominantly driven by microglia in LPS-inflamed mice. Tissue Analysis demonstrates microglial activation.** A) Flow cytometry gating strategy. B) Flow cytometry analyses of microglia ($CD11b^{+}CD45^{lo}$) and peripheral immune cells ($CD45^{hi}$) in single cell suspensions of the brains of control and LPS-inflamed mice. C) IBA1 levels in brain lysates of control and LPS-inflamed mice and immunohistochemical treatment of uninflamed and LPS-inflamed mice using markers for microglia (IBA1) and infiltrating immune cells (Ly6-G/Ly-6C). D) CD45 signal intensity and cell granularity were increased within the microglia population in mice injected with LPS.

## Supplementary Files

This is a list of supplementary files associated with this preprint. Click to download.

- SI5.7.26.docx